Am J Transl Res 2026;18(6):4681-4702
www.ajtr.org /ISSN:1943-8141/AJTR0173071

Original Article

Shenzhu Guanxin formula alleviates atherosclerosis in rats via PI3K/Akt pathway inhibition: a comparative study of decoction and granule forms

Yibei Xie[1*], Cuicui Meng[1*], Shuangmei Li[1*], Zijie Huang[1], Shujun Yang[1], Liying Pei[1], Wan Li[1], Danping Xu[2], Tong Wang[1]

[1]Department of Emergency, The Eighth Affiliated Hospital of Sun Yat-sen University, Shenzhen, Guangdong, P. R. China; [2]Department of Chinese Medicine, The Eighth Affiliated Hospital of Sun Yat-sen University, Shenzhen, Guangdong, P. R. China. [*]Equal contributors.

Received April 3, 2026; Accepted May 11, 2026; Epub June 15, 2026; Published June 30, 2026

Abstract: Shenzhu Guanxin Formula (SGF), a traditional Chinese medicinal compound comprising nine classical herbal constituents, has demonstrated clinical efficacy in the treatment of coronary heart disease. However, its bioactive components and mechanistic underpinnings in atherosclerosis (AS) remain elusive. This study aimed to elucidate the anti-atherosclerotic effects, bioactive constituents, therapeutic targets, and underlying mechanisms of both SGF decoction and granule formulations. An atherosclerotic rat model was established using a 16-week high-fat diet, supplemented with vitamin D_3 injections and carotid artery clamping. The anti-atherosclerotic efficacy of varying doses of SGF granules and decoction was assessed by quantifying serum lipid profiles, antioxidant capacity, inflammatory markers, and vascular morphology. Mechanistic insights were explored by integrating network pharmacology with carotid artery transcriptomics, followed by experimental validation in human umbilical vein endothelial cells (HUVECs) treated with SGF-medicated serum. Results indicated that SGF dose-dependently ameliorated atherosclerotic progression in rats, evidenced by improved serum lipid parameters, reduced carotid plaque burden and arterial/hepatic lipid deposition, enhanced antioxidant status (elevated superoxide dismutase and glutathione levels), and decreased concentrations of interleukin (IL)-6, IL-1β, and tumor necrosis factor-α (TNF-α). Western blot analysis revealed downregulation of phosphorylated Akt (p-Akt), phosphorylated phosphatidylinositol 3-kinase (p-PI3K), vascular endothelial growth factor A (VEGF-A), intercellular adhesion molecule-1 (ICAM-1), and vascular cell adhesion molecule-1 (VCAM-1), along with upregulation of endothelial nitric oxide synthase (eNOS). Integrated network pharmacology and transcriptomic analyses identified 99 putative active components and 243 AS-related targets, highlighting the PI3K-Akt signaling pathway as pivotal. In oxidized low-density lipoprotein (oxLDL)-injured HUVECs, SGF-medicated serum attenuated reactive oxygen species (ROS) generation and suppressed PI3K/Akt activation, thereby supporting the in-silico predictions. In conclusion, both SGF decoction and granule formulations exert comparable anti-atherosclerotic effects in rats, primarily through ameliorating dyslipidemia, inflammation, and plaque burden, largely mediated via inhibition of the PI3K/Akt pathway.

Keywords: Shenzhu Guanxin formula, atherosclerosis, dosage form, PI3K/Akt, network pharmacology

Introduction

Atherosclerosis (AS) represents the principal pathological foundation of cardiovascular diseases, which constitute the foremost cause of global morbidity and mortality [1]. Its pathogenesis is predominantly driven by dyslipidemia-induced endothelial dysfunction, initiating a cascade of lipid deposition, chronic inflammation, oxidative stress, and sustained platelet activation throughout the continuum from lesion formation to thrombotic occlusion [2-4].

In Traditional Chinese Medicine (TCM), AS is attributed to dysfunction of the liver, spleen, and kidney, leading to the accumulation of phlegm and blood stasis [5]. TCM formulations designed to strengthen the spleen, tonify qi, resolve phlegm, and activate blood circulation have demonstrated well-established anti-AS

https://doi.org/10.62347/PADH7084

Table 1. Detailed compositions of SGF

Formula components	Traditional name of the component	Part used	Family of the component	Scientific name of the component	Weight
Ginseng	Renshen	Dried root and rhizome	*Araliaceae*	*Panax ginseng C. A. Mey.*	5 g
Danshen	Danshen	Dried root and rhizome	*Lamiaceae*	*Salvia miltiorrhiza Bge.*	10 g
American Ginseng	Xiyangshen	Dried root	*Araliaceae*	*Panax quinquefolium L.*	5 g
Notoginseng	Sanqi	Dried root and rhizome	*Araliaceae*	*Panax notoginseng (Burk.) F. H. Chen*	5 g
Leech	Shuizhi	Dried whole body	*Hirudinidae*	*Hirudo nipponica Whitman*	3 g
Pinellia Tuber (Prepared)	Fabanxia	Processed product of Pinellia ternata tuber	*Araceae*	*Pinellia ternata (Thunb.) Breit.*	10 g
Largehead Atractylodes Rhizome	Baizhu	Dried rhizome	*Asteraceae*	*Atractylodes macrocephala Koidz.*	10 g
Dried Tangerine Peel	Chenpi	Dried mature pericarp	*Rutaceae*	*Citrus reticulata Blanco*	10 g
Pummelo Peel	Huajuhong	Dried outer layer of pericarp	*Rutaceae*	*Citrus grandis 'Tomentosa' or Citrus grandis (L.) Osbeck*	10 g

efficacy [6-9]. Shenzhu Guanxin Formula (SGF), a patented TCM compound derived from Wendan Decoction and modified by Professor Deng Tietao, is clinically employed for coronary heart disease and platelet hyperactivity [10-13]. Comprising nine medicinal components, SGF exhibits lipid-regulating and antithrombotic properties, with identified bioactive constituents including notoginsenoside R1 and various ginsenosides [14, 15]. Nevertheless, the precise mechanisms underlying its anti-AS effects, particularly in endothelial regulation, remain inadequately elucidated.

Traditional TCM decoctions are constrained by laborious preparation processes and limited portability [16], whereas formula granules - modern (formulations involving single-herb extraction and pre-blending) - offer enhanced convenience and improved quality control [17, 18]. However, the therapeutic equivalence between granules and traditional combined decoctions remains a critical unresolved issue requiring rigorous validation [19].

To date, no direct comparative study has evaluated the anti-AS efficacy and mechanisms of SGF decoction versus granules. Herein, we employed an atherosclerotic rat model to conduct a head-to-head comparison of these two formulations. By integrating transcriptomic profiling of carotid arteries, network pharmacology predictions, and in vitro validation, we systematically elucidated the underlying mechanisms. This study provides novel insights into the therapeutic equivalence of SGF granules and decoction in anti-AS interventions and reveals their core pharmacological mechanisms.

Material and methods

Preparation of SGF

SGF comprises nine natural medicinal ingredients (**Table 1**). All raw Chinese herbal medicines and corresponding formula granules were supplied by Guangdong EFONG Pharmaceutical Co., Ltd., and these materials were inspected by two senior Chinese medicine pharmacists. For the traditional decoction, the nine herbs were accurately weighed in accordance with the formula proportions. They were then immersed in purified water for 30 minutes and boiled in a clay pot for 30 minutes. Subsequently, the mixture was simmered over low heat for 30 minutes, after which the medicinal liquid was filtered and collected. An eightfold volume of water was added to the remaining herb residue, followed by boiling for 15 minutes and filtration. The resulting filtrates were combined and evaporated to a concentration of 1 g/mL using a rotary evaporator (Hei-VAP Core, Heidolph, Germany) to form the decoction solution. The SGF granule formulation was prepared by proportionally dissolving single-ingredient formula granules in purified water and heating the solution to achieve a concentration of 1 g/mL.

Animal experiments

Sprague-Dawley rats (6 weeks; 200 g ± 20 g; male) were obtained from the Zhuhai Bes-Test Bio-Tech Co,. Ltd. (SCXK 2020-0051001). Fifteen rats were used for collecting drug-containing serum for in vitro experiments, while 48 rats were used for in vivo experiments. Rats

were housed in a standardized breeding environment with 12 h light/dark cycle and provided with sufficient food and water. The animal experiments were performed in compliance with the ARRIVE guidelines and approved by the Animal Ethics Committee of The Eighth Affiliated Hospital of Sun Yat-sen University (Approval number: No. 202403301).

Following a one-week acclimatization period, 48 SD rats were randomly divided into eight groups: sham, model, low-/medium-/high-dose traditional decoction (TD-L/TD-M/TD-H), and low-/medium-/high-dose granule (G-L/G-M/G-H) groups. In the sham group, the carotid artery was exposed but not occluded. All other groups underwent 20-min occlusion of the left carotid artery with a vascular clamp, followed by reperfusion. Postoperatively, penicillin (800,000 IU/day) was administered intramuscularly for three consecutive days to all animals. The sham group were maintained on standard chow, while the remaining groups were fed with high-fat feed (containing 36% fat, 0.2% sodium cholate and 1.2% cholesterol). After surgery, all subjects were injected with vitamin D_3 (600,000 IU/kg; cat# 080681417; Harbin Sanma Animal Pharmaceutical, China) through the intraperitoneal route, with subsequent monthly injections of 100,000 IU/kg, while the sham group was given equivalent saline [7].

The dose of gastric infusion was determined by using the body surface area conversion method [20]. The low, medium and high gavage doses (calculated based on the amount of raw drug) were 3.03 $g \cdot kg^{-1} \cdot day^{-1}$, 6.07 $g \cdot kg^{-1} \cdot day^{-1}$ and 12.14 $g \cdot kg^{-1} \cdot day^{-1}$, respectively. All animals were administered their respective formulations by gavage once every two days in 16 weeks.

Preparation of high-concentration medicated serum

Fifteen rats were administered decoction (6.07 g/kg/day), granules (6.07 g/kg/day), and saline. After a 7-day gavage intervention, the rats were euthanized and serum was collected. The serum was heat-inactivated in a 56°C water bath for 30 minutes, then filtered through 0.22 μm membranes, aliquoted into several equal portions, and finally stored in an ultra-cold freezer at -80°C.

Sample collection

Following a one-week acclimatization period, blood was collected from the retro-orbital plexus. At week 16, carotid ultrasound was performed under 2% isoflurane anesthesia; animals were then euthanized by exsanguination under deep anesthesia. Kidney, heart, liver, aorta and carotid artery were collected for subsequent analysis. The organ index was calculated as organ weight (mg) divided by body weight (g).

Histopathology

Carotid artery specimens were fixed in 10% neutral buffered paraformaldehyde for 24 h, followed by standard gradient dehydration, paraffin infiltration and embedding. Tissues were sectioned into 4-6 μm slices, deparaffinized with xylene, and stained with hematoxylin and eosin (H&E) using a commercial kit (Cat# G1076, Servicebio, China). Images were acquired from three random visual fields per section under an upright optical microscope (Nikon Eclipse C1, Japan). Carotid intima-media thickness (CIMT) was measured using ImageJ software (Java 13.0.6, USA).

For assessment of lipid deposition, rat carotid artery and liver samples were fixed, embedded in OCT compound, and processed for cryosectioning. Subsequent staining with Oil Red O was performed on these sections (Cat# G1015, Servicebio, China). ImageJ software was used to calculate the proportion of lipid area in the total tissue area.

Ultrasound imaging of carotid artery

Rats were anesthetized with 2% isoflurane and carotid arteries were examined using a small animal ultrasound imaging device (Vevo 2100, Visualsonics, Canada). The operator was blinded to the animal grouping. The carotid artery wall thickness, peak systolic velocity (PSV), end-diastolic velocity (EDV), plaque size and vascular stenosis were evaluated.

Detection of serum biochemical index

Low-density lipoprotein cholesterol (LDL-C), total cholesterol (TC), high-density lipoprotein cholesterol (HDL-C), and triglycerides (TG) levels in serum were detected using reagent

kits from Elabscience Biotechnology (Wuhan, China). Glutathione (GSH) and superoxide dismutase (SOD) levels were measured using reagent kits from Beyotime Biotechnology and Nanjing Jiancheng Bioengineering Institute.

Enzyme-linked immunosorbent assay (ELISA)

IL-1β, IL-6 and TNF-α levels in serum were determined by ELISA kits (Cat# E-HSEL-R0002; Cat# E-EL-M0044; Cat# E-EL-R0019c) from Elabscience Biotechnology Co., Ltd.

Transcriptome sequencing and analysis

Five replicates were included for each of the sham, model group, decoction (high dose) and granule group (high dose). Carotid artery tissues were sent to Beijing Novogene for transcriptome sequencing. Differentially expressed genes (DEGs) were identified using the DESeq2 software; genes with p-value < 0.05 and |log2 fold change| > 1 were selected. In addition, Kyoto Encyclopedia of Genes and Genomes (KEGG) pathway enrichment analysis and Gene Ontology (GO) functional enrichment analysis were conducted, with p-value < 0.05 as the enrichment threshold.

Network pharmacology analysis

Collection of active ingredients and targets of SGF components: The active ingredients of SGF were screened under the conditions of oral bioavailability > 30% and drug-likeness > 0.18 based on the TCMSP database. The compound components contained in "*Ginseng*", "*Atractylodes Macrocephala*", "*Notoginseng*", "*Pinellia Ternata*", "*American Ginseng*", "*Tangerine Peel*", "*Exocarpium Citri Grandis*", and "*Salvia Miltiorrhiza*" were retrieved from TCMSP. Literature sources were consulted, and the chemical components of "Hirudo" were retrieved from the Herb database. By searching the PubChem platform, we obtained the matching SMILES codes. Subsequently, compounds were screened using the SwissADME platform to identify compounds with high gastrointestinal absorption (GI absorption) and those that met at least two of the five rules proposed by Egan, Veber, Ghose, Muegge, and Lipinski, enabling the prediction of SGF active ingredients. Next, we utilized the SwissTargetPrediction platform to predict the effective component targets of the aforementioned TCM, and set the predicted probability threshold to > 0. We then sorted the prediction results to eliminate duplicate targets.

Screening of atherosclerosis targets: The DisGeNET database, OMIM database and GeneCards database were searched using "atherosclerosis" as the keyword. The targets of atherosclerosis were obtained after removing duplicates.

Analysis of the association between disease targets and drugs: The targets of atherosclerosis were intersected with those of SGF to obtain the anti-atherosclerotic targets of SGF. To obtain the interaction relationships between these targets, they were imported into the STRING database. The "minimum required interaction score" was set to ≥ 0.400, the species was selected as "Homo sapiens", and other parameters were set to default. Finally, the Cytoscape software (3.10.3) was used to construct a protein-protein interaction (PPI) network. Subsequently, the Centiscape 2.2 plugin was employed to screen for key target points. Within the plugin, the Degree, Closeness, and Betweenness algorithms were selected, resulting in the identification of key target nodes.

Gene enrichment analysis: To annotate the gene functions, GO enrichment analysis, containing Biological Process (BP), Cellular Component (CC), Molecular Function (MF) and KEGG signal pathway enrichment analysis was performed through the Metascape database.

Experimental cells

Human umbilical vein endothelial cells (HUVECs) were acquired from Zhongqiao Xinzhou Biotechnology Co., Ltd., while trypsin and phosphate-buffered saline were sourced from Thermo Fisher Scientific (Beijing, China). Fetal bovine serum, endothelial cell culture medium, penicillin-streptomycin (100×), and endothelial cell growth factor were sourced from ScienCell. The incubator was set at a constant temperature of 37°C with 95% humidity and 5% CO_2. Medium was replaced every 48 h, and cells were passaged with 0.25% trypsin upon reaching 90% confluence.

CCK-8 and reactive oxygen species (ROS) assay

Cell proliferation was detected using a CCK-8 kit. HUVECs seeded in 96-well plates were

treated with oxidized low-density lipoproteins (oxLDL) (Yiyuan Biotechnology, China) for 24 h, followed by treatment with or without drug-containing serum for an additional 24 h. Then, CCK-8 reagent (DOJINDO, Japan) (10 μL/well) was added and incubated for 1 h before measuring absorbance at 450 nm.

ROS levels were detected according to the standard procedure in the instruction manual of the ROS detection kit (Beyotime Biotechnology). After 24 hours of oxLDL treatment, cells were cultured with drug-containing serum and/or Sc79 (an agonist of Akt, Beyotime Biotechnology), then incubated in the dark for 25 minutes after the addition of DCFH-DA. Images were captured under an upright fluorescence microscope (Axio Observer 7, ZEISS, Germany) using an excitation wavelength of 488 nm.

Western blotting

The protein concentrations of arterial tissues and cells were determined using the BCA kit. Western blotting was performed to detect the expression of vascular endothelial growth factor (VEGF-A), intercellular adhesion molecule (ICAM-1), endothelial nitric oxide synthase (eNOS), vascular cell adhesion molecule (VCAM-1), phosphorylated Threonine Kinase (p-Akt), phosphorylated phosphatidylinositol 3-Kinase (p-PI3K), Akt and PI3K proteins. The following antibodies were used: GAPDH Monoclonal antibody (Cat No.60004-1-Ig) and VEGFA Polyclonal antibody (Cat#26157-1-AP) were purchased from Proteintech Technology; VCAM-1 Rabbit PolymAb (Cat#A19131PM) and ICAM-1/CD54 Rabbit mAb (Cat# A24648) were purchased from ABclonal Technology; Anti-PI 3 Kinase p85 alpha (phospho Y467) + PI3 Kinase p55 (phospho Y199) antibody (Cat# ab278545) was purchased from Abcam; eNOS (D9A5L) Rabbit mAb (Cat# 32027), Akt Antibody (Cat# 9272), PI3 Kinase p85 Antibody (Cat# 4292), Phospho-Akt (Ser473) Rabbit mAb antibody (Cat# 4060S) and Anti-rabbit IgG HRP-linked Antibody (Cat# 7074S) were purchased from Cell Signaling Technology. Band intensities were measured using ImageJ software (Java 13.0.6).

Statistical analysis

Data analysis and graph generation were performed using SPSS version 27.0.1.0 and GraphPad Prism version 10.3.1. The Shapiro-Wilk test was applied to assess the normality of measurement data. Data conforming to a normal distribution were presented as mean ± SD. For data with homogeneous variances, one-way ANOVA followed by LSD post hoc test was used for multiple comparisons. For data with heterogeneous variances, Tamhane's T2 post-hoc test was adopted for multiple pairwise comparisons. All statistical tests were two-sided, and P < 0.05 was considered statistically significant.

Results

Effects of SGF on organ indices in atherosclerotic rats

In the analysis of organ indices, compared with the sham group, the heart, liver, and kidney weight indices were significantly increased in atherosclerotic model rats ($P < 0.001$, **Table 2**). SGF treatment significantly reduced the kidney index ($P < 0.001$) and heart index relative to the model group ($P < 0.01$). Significant improvements in liver indices were seen in the high dose ($P < 0.001$) and medium dose groups ($P < 0.01$) (**Table 2**). No statistically significant differences were observed between granule and decoction formulations ($P > 0.05$).

Effects of SGF on serum lipoproteins in atherosclerotic rats

At week 16, the model group exhibited higher LDL-C, TC, and TG levels and lower HDL levels compared with the sham group (all $P < 0.001$; **Table 2**). All SGF doses significantly reduced TC and TG ($P < 0.01$ vs. model). High- and medium-dose groups had significantly increased HDL ($P < 0.001$) and decreased LDL-C ($P < 0.001$). The low-dose groups did not significantly affect HDL or LDL-C ($P > 0.05$).

Effects of SGF on serum biochemical indicators in atherosclerotic rats

The model group showed higher IL-1β, IL-6, and TNF-α concentrations and lower GSH and SOD levels compared with the sham group (all $P < 0.01$; **Table 3**). Low-dose SGF did not significantly alter TNF-α or SOD levels ($P > 0.05$). All SGF doses significantly reduced IL-6 ($P < 0.001$) and increased GSH ($P < 0.05$). IL-1β ($P < 0.05$) and TNF-α levels ($P < 0.01$) were numerically lower in low or medium dose granule groups than in corresponding decoction groups.

Table 2. Effect of SGF on organ index and serum lipid levels in atherosclerotic rats ($\bar{x}$±s, n=6)

Group	Kidney Index/ (mg·kg^{-1})	Heart Index/ (mg·kg^{-1})	Liver Index/ (mg·kg^{-1})	TC/(mmol·L^{-1})	TG/(mmol·L^{-1})	HDL-C/(mmol·L^{-1})	LDL-C/(mmol·L^{-1})
Sham	3.40±0.72***	1.63±0.32***	17.90±2.97***	3.03±0.55***	1.14±0.02***	0.94±0.04***	0.89±0.10***
Model	8.84±1.81$^{\#\#\#}$	3.56±0.57$^{\#\#\#}$	49.59±9.52$^{\#\#\#}$	4.35±0.09$^{\#\#\#}$	2.83±0.09$^{\#\#\#}$	0.50±0.04$^{\#\#\#}$	2.15±0.13$^{\#\#\#}$
TD-H	4.51±0.82$^{***,\#}$	1.81±0.43***	27.38±6.41$^{***,\#}$	3.17±0.08***	1.25±0.18***	0.91±0.01***	1.05±0.04***
G-H	3.40±0.63***	1.72±0.35***	21.04±3.61***	3.16±0.18***	1.22±0.09***	0.88±0.07$^{***,\#}$	0.92±0.06***
TD-M	5.38±0.85$^{***,\#\#}$	2.39±0.38$^{***,\#\#\#}$	37.47±4.64$^{**,\#\#\#}$	3.33±0.09$^{***,\#\#\#}$	1.97±0.07$^{***,\#\#\#}$	0.81±0.06$^{***,\#\#\#}$	1.47±0.03$^{***,\#\#\#}$
G-M	4.73±0.57$^{***,\#}$	2.38±0.27$^{***,\#\#\#}$	33.17±7.99$^{***,\#\#\#}$	3.28±0.06$^{***,\#\#}$	1.67±0.13$^{***,\#\#}$	0.81±0.04$^{***,\#\#\#}$	1.42±0.05$^{***,\#\#\#}$
TD-L	6.15±0.48$^{***,\#\#\#}$	2.79±0.20$^{***,\#\#\#}$	43.09±6.96$^{\#\#\#}$	4.09±0.15$^{***,\#\#\#}$	2.29±0.17$^{**,\#\#\#}$	0.52±0.04$^{\#\#\#}$	1.87±0.07$^{\#\#\#}$
G-L	6.20±0.89$^{***,\#\#\#}$	2.95±0.18$^{**,\#\#\#}$	36.76±9.45$^{**,\#\#\#}$	4.01±0.18$^{***,\#\#\#}$	2.47±0.10$^{**,\#\#\#}$	0.46±0.06$^{\#\#\#}$	1.88±0.07$^{\#\#\#}$

Note: The serum levels of TC, TG, HDL and LDL-C were evaluated in 16th week. Compared to the Model group: $^{**}P < 0.01$, $^{***}P < 0.001$; compared to the Sham group: $^{\#}P < 0.05$, $^{\#\#}P < 0.01$, $^{\#\#\#}P < 0.001$. TD-H, TD-M, TD-L: High/Medium/Low dose traditional decoction of SGF. G-H, G-M, G-L: High/Medium/Low dose granule of SGF.

Table 3. SGF significantly reduced oxidative stress and inflammatory damage in atherosclerotic rats ($\bar{x}$±s, n=6)

Group	IL-1β/(pg·ml^{-1})	IL-6/(pg·ml^{-1})	TNF-α/(pg·ml^{-1})	GSH/(mmol·L^{-1})	SOD/(U·ml^{-1})
Sham	53.11±8.34**	29.00±6.59***	84.37±12.85***	365.20±63.54***	8.63±1.34**
Model	565.43±142.65$^{\#\#}$	346.23±50.16$^{\#\#\#}$	551.34±68.63$^{\#\#\#}$	90.03±21.55$^{\#\#\#}$	2.46±0.32$^{\#\#}$
TD-H	90.41±12.55$^{**,\#\#}$	85.98±45.50$^{***,\#\#}$	226.83±79.86***	259.75±25.80***	6.32±1.43*
G-H	88.20±16.64**	68.64±30.94$^{***,\#}$	219.67±33.90$^{***,\#\#}$	265.39±28.32***	6.21±1.17*
TD-M	135.41±19.375$^{*,\#\#\#}$	148.37±26.35$^{***,\#\#\#}$	423.54±60.19$^{\#\#\#}$	186.55±20.55$^{***,\#}$	4.56±0.68$^{**,\#\#}$
G-M	123.28±13.32$^{*,\#\#\#}$	151.09±21.33$^{***,\#\#\#}$	351.93±41.06$^{**,\#\#\#}$	203.68±17.82$^{***,\#}$	4.41±0.51$^{***,\#\#}$
TD-L	270.24±42.94$^{\#\#}$	274.65±20.02$^{***,\#\#\#}$	496.65±67.15$^{\#\#\#}$	133.16±17.78$^{*,\#\#}$	2.91±0.41$^{\#\#}$
G-L	245.94±60.24$^{*,\#}$	274.80±24.09$^{***,\#\#\#}$	436.38±90.58$^{\#\#}$	130.19±15.75$^{*,\#\#}$	3.16±0.38$^{\#\#}$

Note: Compared to the Model group: $^{*}P < 0.05$, $^{**}P < 0.01$, $^{***}P < 0.001$; compared to the Sham group: $^{\#}P < 0.05$, $^{\#\#}P < 0.01$, $^{\#\#\#}P < 0.001$. TD-H, TD-M, TD-L: High/Medium/Low dose traditional decoction of SGF. G-H, G-M, G-L: High/Medium/Low dose granule of SGF.

Carotid artery ultrasound findings after treatment with SGF

Carotid ultrasound revealed smooth arterial walls in the sham group, while the atherosclerosis group exhibited markedly thickened and rough intimal surfaces, along with protruding spots and distinct raised plaques. SGF treatment alleviated atherosclerosis-related pathological changes, including arterial wall thickening and hardened spots (**Figure 1**). High- and medium-dose SGF significantly increased PSV and EDV ($P < 0.05$; **Table 4**) and reduced wall thickness ($P < 0.05$; **Table 4**), with the high-dose groups showing the greatest improvement ($P < 0.01$; **Table 4**). No significant differences were found between granule and decoction groups ($P > 0.05$; **Table 4**).

The pathological section results of the left carotid arteries and liver

H&E staining revealed that the model group had significantly increased carotid intima media thickness (CIMT) compared with the sham group ($P < 0.05$; **Table 5**). High-dose SGF markedly reduced CIMT ($P < 0.05$; **Table 5**), with intact endothelial layer and normal media (**Figure 2A**). Medium-dose groups showed partial improvement with residual vacuolization and smooth muscle proliferation ($P < 0.05$; **Table 5**). Low-dose groups displayed limited improvement ($P > 0.05$; **Table 5**). Oil red O staining demonstrated that SGF dose-dependently decreased the relative lipid-positive area in carotid arteries ($P < 0.05$ for High, medium dose groups; **Figure 2B**) and hepatic lipid accumulation ($P < 0.01$ for all doses; **Figure 2C**). No significant differences were detected between decoction and granule forms ($P > 0.05$).

Effects of SGF on protein levels of VCAM-1, ICAM-1, eNOS and VEGF-A in atherosclerotic rats

Western blot analysis revealed that, compared with the sham group, the protein expression

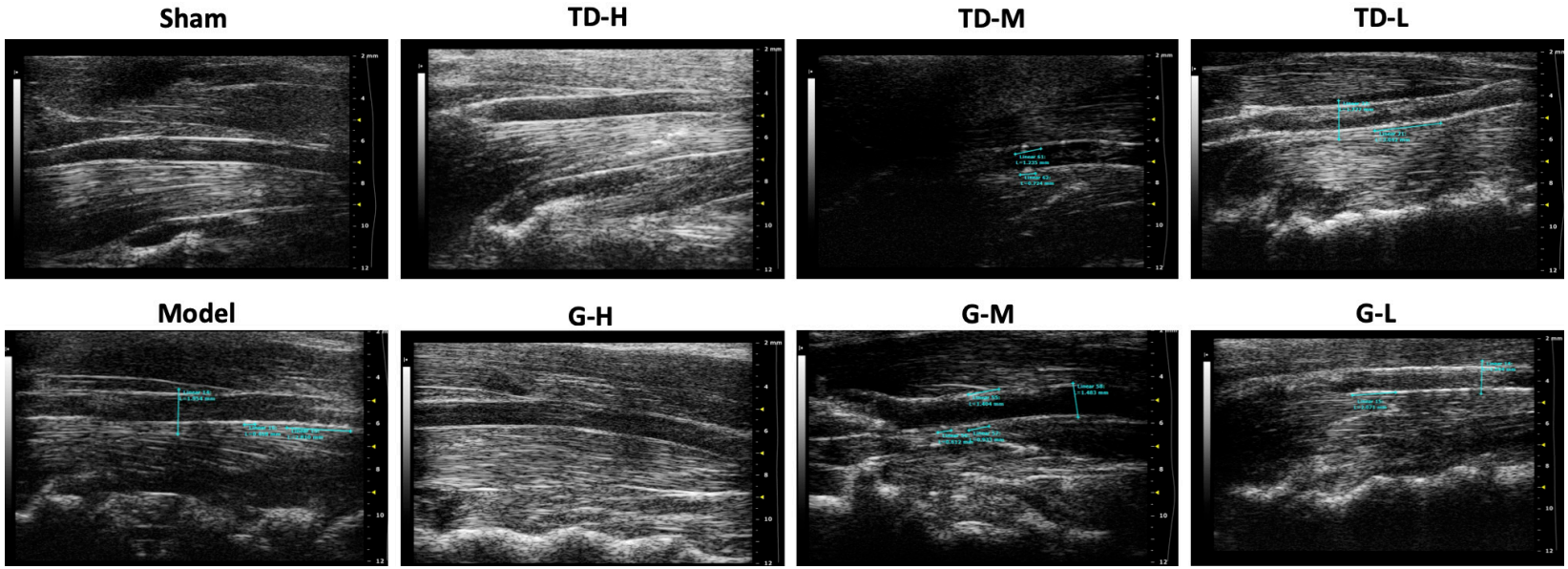

Figure 1. Ultrasonic images of carotid arteries in rats of each group after SGF treatment. Note: The green horizontal line area in the figure is the atherosclerotic plaque of the vessel wall.

Table 4. Quantitative analysis results of PSV, vessel wall thickness and EDV in each group ($\bar{x}$±s, n=6)

Group	PSV/(mm·s^{-1})	EDV/(mm·s^{-1})	vessel wall thickness/(mm)
Sham	2426.74±164.80***	557.15±72.89***	0.13±0.02***
Model	1026.73±91.43$^{\#\#\#}$	188.51±68.74$^{\#\#\#}$	0.20±0.02$^{\#\#\#}$
TD-H	2048.94±172.77***	381.38±66.65$^{***,\#\#\#}$	0.15±0.01***
G-H	2290.85±381.51**	430.68±60.87$^{***,\#\#\#}$	0.14±0.02***
TD-M	1592.50±394.71*	311.83±69.43$^{**,\#\#\#}$	0.17±0.01$^{**,\#\#}$
G-M	1720.19±239.25$^{**,\#\#}$	319.29±63.77$^{***,\#\#\#}$	0.16±0.02$^{***,\#}$
TD-L	1350.09±265.96$^{\#\#\#}$	188.87±44.32$^{\#\#\#}$	0.18±0.01$^{*,\#\#\#}$
G-L	1322.87±206.61$^{\#\#\#}$	184.17±28.13$^{\#\#\#}$	0.18±0.03$^{*,\#\#\#}$

Note: PSV, peak systolic velocity; EDV, end diastolic velocity. Compared to the Model group: $^{*}P < 0.05$, $^{**}P < 0.01$, $^{***}P < 0.001$; compared to the Sham group: $^{\#}P < 0.05$, $^{\#\#}P < 0.01$, $^{\#\#\#}P < 0.001$. TD-H, TD-M, TD-L: High/Medium/Low dose traditional decoction of SGF. G-H, G-M, G-L: High/Medium/Low dose granule of SGF.

Table 5. The semi-quantification results of carotid intima-media thickness of the carotid artery and oil red O-stained area in carotid arteries and liver ($\bar{x}$±s, n=6)

Group	CIMT	oil red O staining area of carotid artery (%)	oil red O staining area of liver
Sham	1.00±0.07*	0.95±0.72$^{\#}$	1.00±0.20***
Model	3.30±0.95$^{\#}$	47.23±14.34	3.21±0.05$^{\#\#\#}$
TD-H	1.28±0.12$^{*,\#}$	4.04±1.19$^{*,\#}$	2.04±0.09$^{***,\#\#\#}$
G-H	1.25±0.10$^{*,\#}$	2.62±1.79$^{*,\#}$	1.79±0.28$^{**,\#\#}$
TD-M	1.52±0.06$^{*,\#\#\#}$	9.16±3.96*	2.49±0.07$^{***,\#\#\#}$
G-M	1.47±0.09$^{*,\#\#\#}$	6.16±2.32*	2.37±0.04$^{***,\#\#\#}$
TD-L	1.76±0.21$^{\#\#}$	24.03±9.82	2.87±0.11$^{**,\#\#\#}$
G-L	1.73±0.18$^{\#\#\#}$	20.95±7.34$^{\#}$	2.73±0.06$^{***,\#\#\#}$

Note: CIMT, carotid intima-media thickness. Compared to the Model group: $^{*}P < 0.05$, $^{**}P < 0.01$, $^{***}P < 0.001$; compared to the Sham group: $^{\#}P < 0.05$, $^{\#\#}P < 0.01$, $^{\#\#\#}P < 0.001$. TD-H, TD-M, TD-L: High/Medium/Low dose traditional decoction of SGF. G-H, G-M, G-L: High/Medium/Low dose granule of SGF.

levels of VCAM-1, ICAM-1, and VEGF-A were significantly increased (**Figure 3A**), while the eNOS ratio was significantly downregulated (**Figure 3B**) in the atherosclerotic model rats. The high-dose groups of both decoction and granules significantly downregulated the expression of VCAM-1, ICAM-1, and VEGF-A (**Figure 3C-E**), while significantly increasing the level of eNOS protein. Although low- and medium-dose SGF exhibited similar trends in their effects, these changes were not statistically significant. In addition, the therapeutic effects of the granule groups and the decoction groups were comparable.

Transcriptome sequencing analysis

Using a threshold of $P < 0.05$ and $|\log_2 FC| \geq 1$, we identified 575 and 493 DEGs in the high-dose SGF granule and decoction groups versus the model group, respectively (**Figure 4A**). Hierarchical clustering heatmaps of core AS-related genes showed that pro-inflammatory *IL6* and PI3K/Akt pathway genes (*Akt1*, *Pik3r1*) were downregulated, while endothelial protective *Nos3* and antioxidant *Sod1* were upregulated by TD-H and G-H treatment (**Figure 4B**). GO analysis showed that DEGs in both treatment groups were prominently enriched in lipid metabolism processes, including triglyceride, neutral lipid, and fatty acid metabolic pathways, providing a transcriptional basis for the observed improvement in dyslipidemia. Extracellular matrix (ECM) components and collagen-related terms were also highly enriched, suggesting regulation of plaque fibrosis and stability. Additionally, terms related to blood vessel morphogenesis and leukocyte-mediated cytotoxicity indicate effects on vascular remodeling and inflammatory cell activity (**Figure 4C**). KEGG analysis identified the PI3K/Akt signaling pathway as a key enriched term, with 30 and 23 DEGs from the decoction and granule groups annotated to this pathway, respectively (**Figure 4D**).

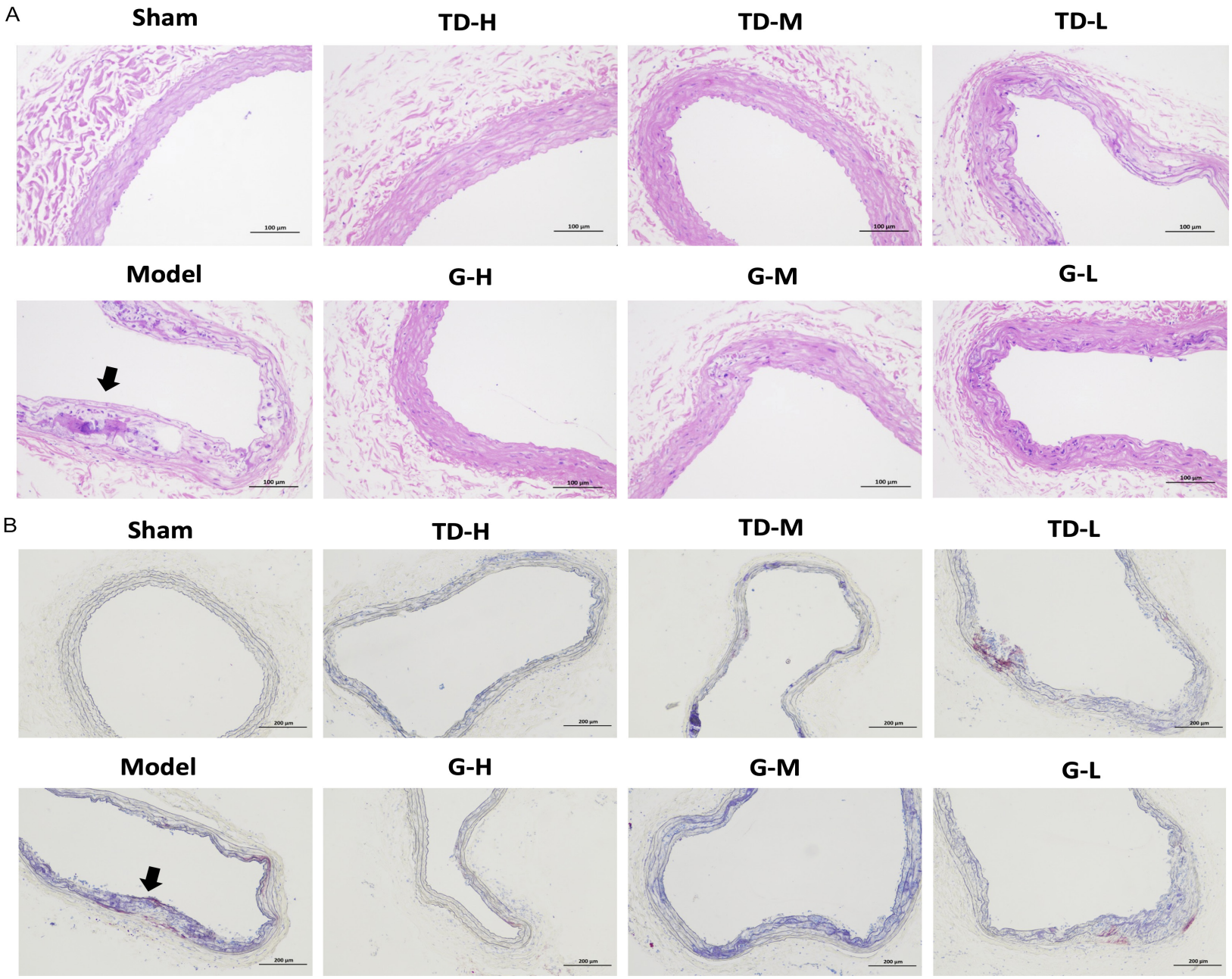
A
Sham
TD-H
TD-M
TD-L
Model
G-H
G-M
G-L
B
Sham
TD-H
TD-M
TD-L
Model
G-H
G-M
G-L

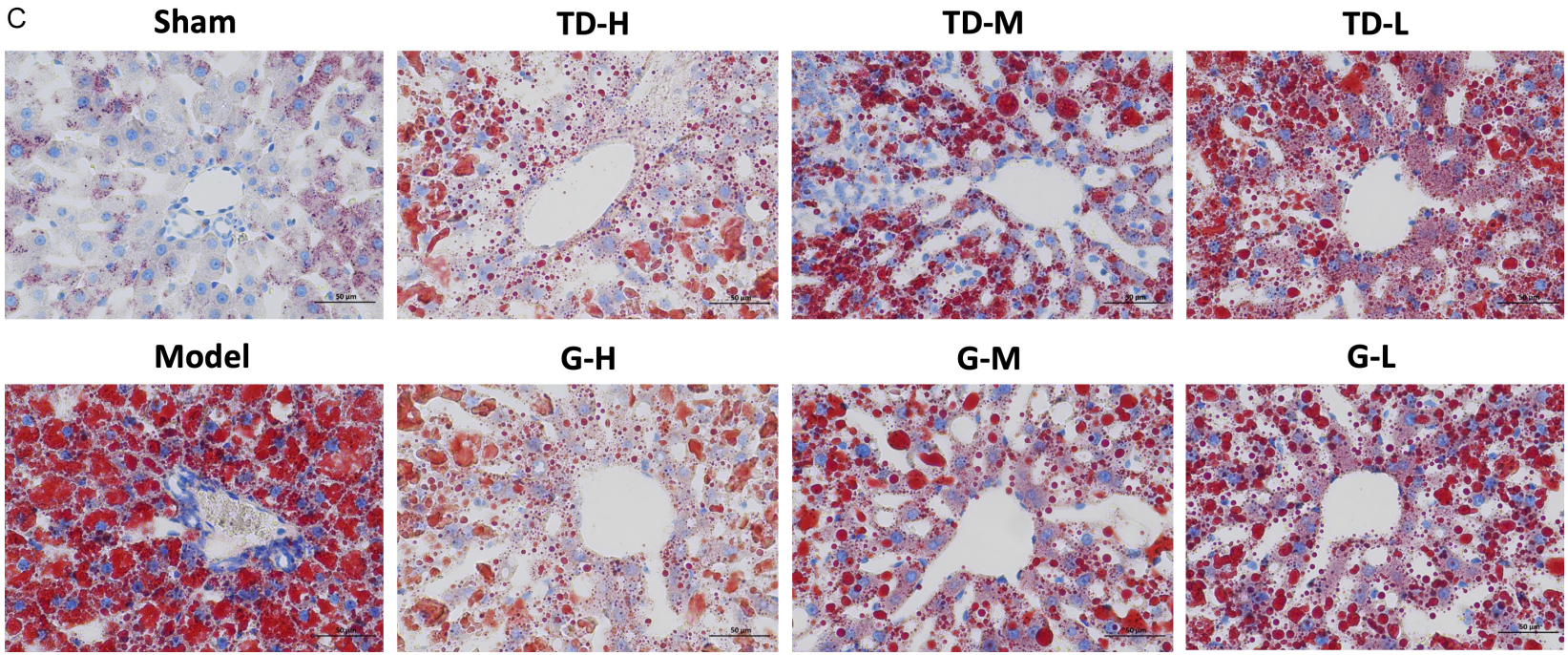

Figure 2. SGF can ameliorate endothelial injuries, reduce carotid and liver lipid deposition in rats with atherosclerosis. A. H&E Staining of the left carotid arteries of the rats after 16-week treatment (200× magnification) and determination of carotid intima-media thickness (CIMT). The arrow indicated endothelial cell thickening and endothelial rupture, accompanied by disordered smooth muscle cell arrangement or calcification. B. Optical microscope image of oil red O staining of rat carotid artery (100× magnification). The area indicated by the black arrow shows red lipid deposits and purple calcification. C. Optical microscope image of liver oil red O staining (400× magnification).

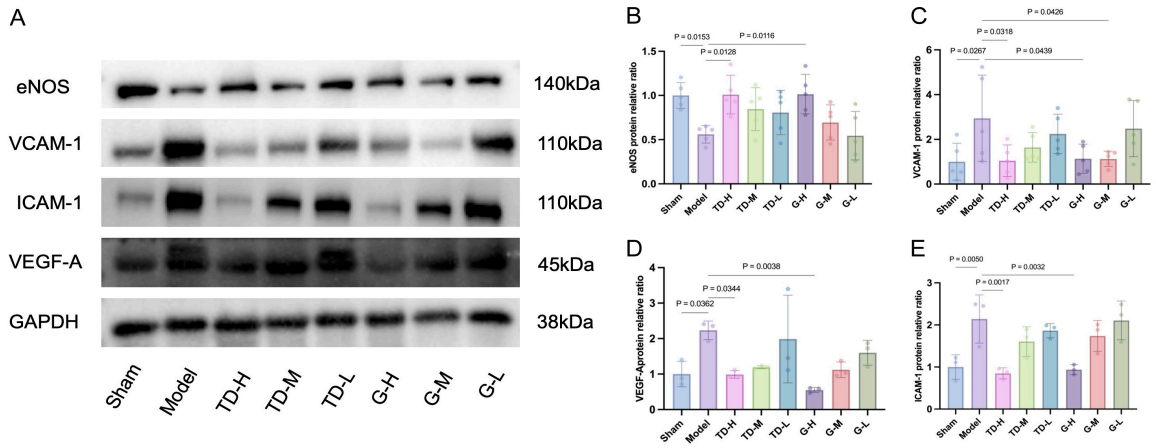

Figure 3. SGF reduced protein expression levels of VCAM-1, VEGF-A, and ICAM-1 and increased protein expression levels of eNOS in arteries. A. Representative images of eNOS, VCAM-1, VEGF-A and ICAM-1. B-E. Protein semi-quantitative analysis normalized to internal references ($\bar{x} \pm s$, n=6). eNOS, endothelial nitric oxide synthase; VCAM-1, vascular cell adhesion molecule-1; VEGF-A, vascular endothelial growth factor-A; ICAM-1, intercellular adhesion molecule-1. TD-H, TD-M, TD-L: High/Medium/Low dose traditional decoction of SGF. G-H, G-M, G-L: High/Medium/Low dose granule of SGF.

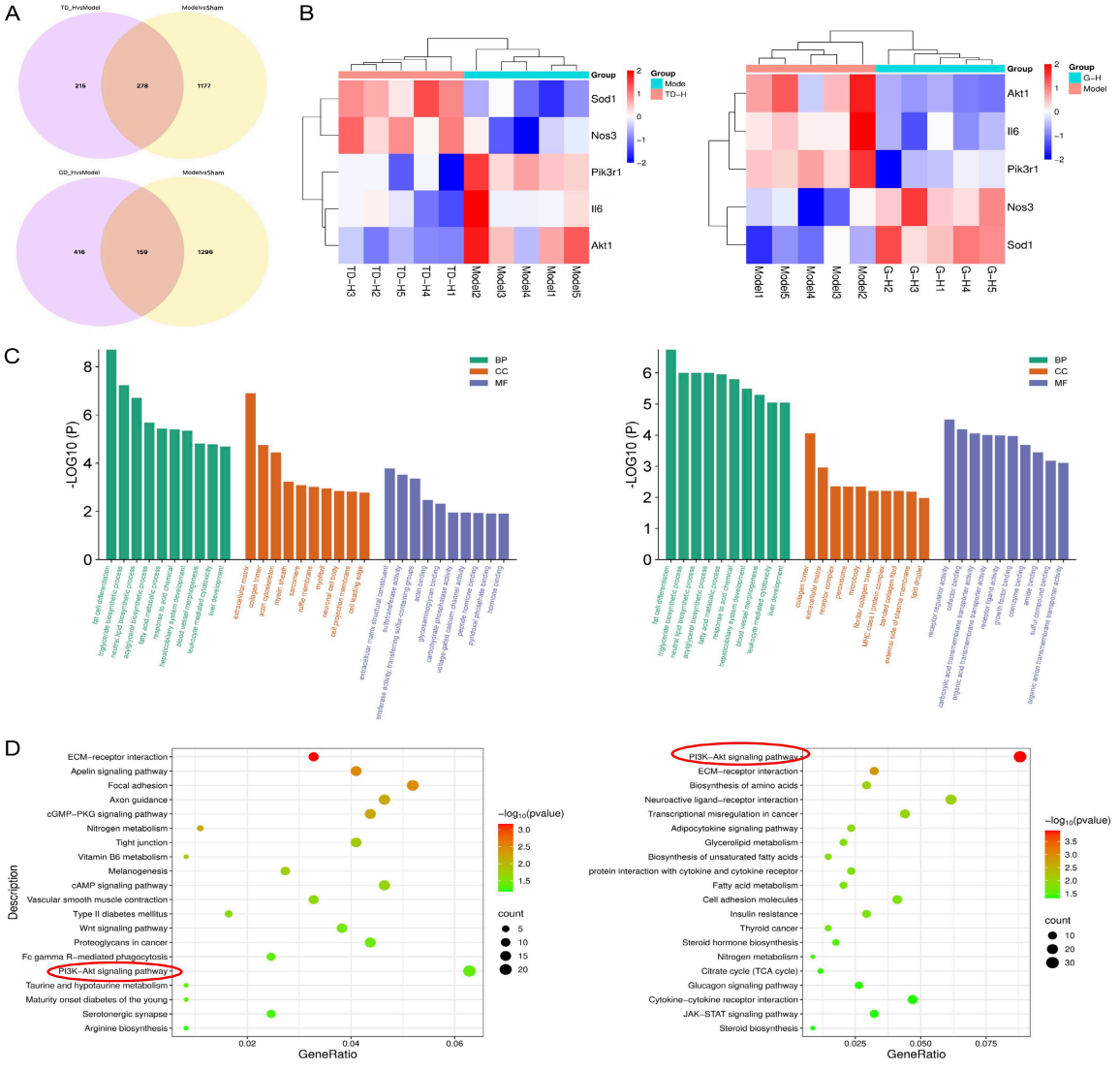

Figure 4. Transcriptome sequencing results. A. Venn diagram of the three groups of DEGs. B. Hierarchical clustering heatmap of core atherosclerotic-related genes in the high-dose SGF decoction group (TD-H) and the model group (left figure), and in the high-dose SGF granule group (G-H) and the model group (right figure). The heatmap shows Z-score normalized mRNA expression of representative genes associated with inflammation, PI3K/Akt signaling, endothelial function, and antioxidant defense. Red indicates upregulated expression, and blue indicates downregulated expression. Each column represents an individual rat sample, and each row represents a target gene. C. GO enrichment analysis. GO analysis was conducted on the DEGs between the high-dose decoction group (left figure) and the model group, as well as between the high-dose granule group (right figure) and the model group. The ten most significant GO terms across BP, MF, and CC were identified. D. KEGG pathway enrichment analysis was performed on DEGs comparing the high-dose decoction group (left) and high-dose granule group (right) against the model group. The results show the top 20 enriched pathways, all of which include the PI3K-Akt pathway.

Network pharmacology results

Through database search, we finally obtained 99 candidate active ingredients (**Appendix 1**). Subsequently, the targets of these ingredients were predicted, and after removing duplicates, 654 unique targets were obtained. By searching and screening the GeneCards, DisGeNET and OMIM databases, 1,259 atherosclerosis targets were obtained. The intersection of these disease targets with the predicted targets of SGF identified 243 potential targets for SGF against atherosclerosis (**Figure 5A**). A total of 243 potential therapeutic targets associated with atherosclerosis were included in the STRING database, and the results were visualized as a PPI network using Cytoscape (**Figure 5B**). Subsequent analysis identified 60 key targets (**Figure 5C**).

After meeting the screening criteria of $P < 0.01$, there were 2,482, 138, and 291 terms in the GO-BP, GO-CC, and GO-MF, respectively, and 219 terms in the KEGG pathway. GO enrichment analysis demonstrated that the most prominent terms were associated with inflammation (regulation of inflammatory response), leukocyte migration (positive regulation of cell migration), vascular processes (circulatory system process), along with kinase- and integrin-binding activities (**Figure 5D**). KEGG pathway analysis further revealed that "Lipid and atherosclerosis", "Fluid shear stress and atherosclerosis", and the TNF, MAPK, and PI3K-AKT signaling pathways were among the most significantly enriched (**Figure 5E**). These pathways directly link SGF targets to lipid-driven inflammation, endothelial mechanotransduction, and key inflammatory cascades that regulate plaque formation and stability. Combined with the results of previous transcriptome KEGG analysis, this convergent finding from two orthogonal approaches - together with the pathway's established roles in endothelial dysfunction, lipid metabolism, and vascular inflammation - provided a clear rationale for selecting PI3K/Akt as the key candidate mechanism for subsequent experimental validation.

Effects of SGF on key proteins in the PI3K/Akt pathway in the atherosclerotic rats

The images semi-quantitative analysis results of the western blot showed that, compared with the sham operation group, the ratios of p-PI3K/PI3K and p-Akt/Akt in the arterial tissue of the atherosclerotic model rats was significantly increased ($P < 0.001$; **Figure 6A**). The levels of p-PI3K/PI3K ($P < 0.001$) and p-Akt/Akt ($P < 0.05$) were significantly decreased in the high-dose SGF group (**Figure 6B**, **6D**), but the protein levels of PI3K and Akt were not changed (**Figure 6C**, **6E**). Collectively, atherosclerosis activated PI3K/Akt signaling via transcriptional upregulation and increased protein phosphorylation, without affecting total protein content. SGF effectively restrained this pathological activation by reversing both gene upregulation and PI3K/Akt hyperphosphorylation.

SGF ameliorated the reduction in HUVEC viability and the generation of intracellular ROS induced by oxLDL

To evaluate the safety of drug serum *in vitro*, we exposed HUVECs to different concentrations of SGF. After 24 hours, 5% and 10% SGF-medicated serum enhanced the activity of HUVECs ($P < 0.0001$; **Figure 7A**). Additionally, oxLDL significantly reduced the activity of HUVECs in a dose-dependent manner ($P < 0.05$; **Figure 7B**). We treated HUVECs for 24 hours with 5% and 10% SGF drug-containing serum and 75 μg/mL oxLDL, and SGF significantly alleviated oxLDL-induced cell viability damage caused by oxLDL ($P < 0.05$; **Figure 7C**).

ROS fluorescence staining showed that SGF-medicated serum inhibited oxLDL-induced ROS

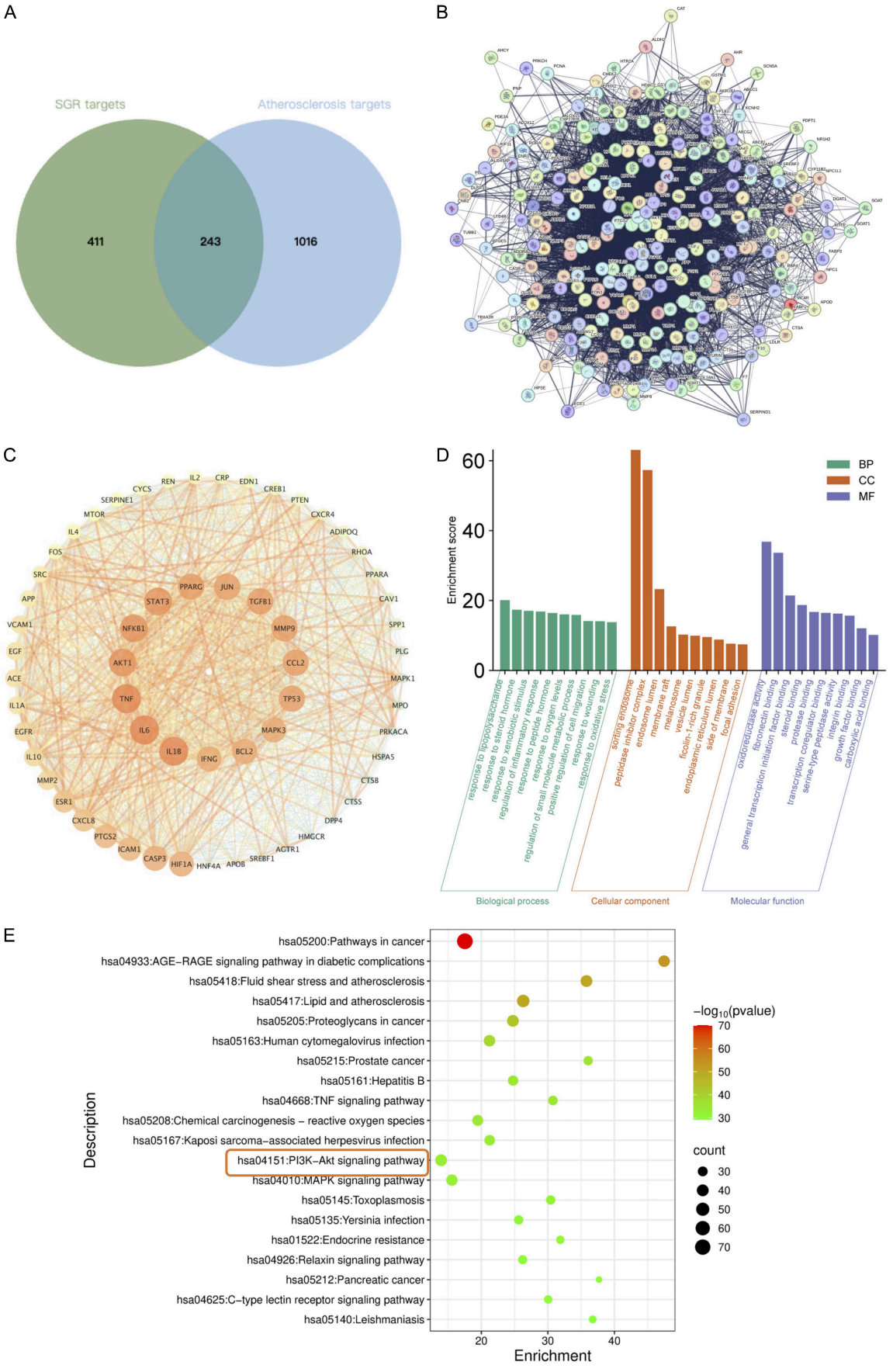
A
SGR targets
Atherosclerosis targets
411
243
1016
B
C
REN
IL2
CRP
EDN1
CYCS
CREB1
SERPINE1
PTEN
MTOR
CXCR4
IL4
ADIPOQ
FOS
RHOA
SRC
PPARA
PPARG
JUN
APP
STAT3
TGFB1
CAV1
VCAM1
NFKB1
MMP9
SPP1
EGF
AKT1
CCL2
PLG
ACE
TNF
TP53
MAPK1
IL1A
MPO
EGFR
IL6
MAPK3
PRKACA
IL10
IL1B
IFNG
BCL2
HSPA5
MMP2
CTSB
ESR1
CTSS
CXCL8
DPP4
PTGS2
HMGCR
ICAM1
ACTR1
CASP3
HIF1A
HNF4A
APOB
SREBF1
D
Enrichment score
60
40
20
0
BP
CC
MF
response to lipopolysaccharide
response to steroid hormone
response to xenobiotic stimulus
regulation of inflammatory response
response to peptide hormone
response to oxygen levels
regulation of small molecule metabolic process
positive regulation of cell migration
response to wounding
response to oxidative stress
sorting endosome
peptidase inhibitor complex
endosome lumen
membrane raft
melanosome
vesicle lumen
ficolin-1-rich granule
endoplasmic reticulum lumen
side of membrane
focal adhesion
oxidoreductase activity
fibronectin binding
general transcription initiation factor binding
steroid binding
protease binding
transcription coregulator binding
serine-type peptidase activity
integrin binding
growth factor binding
carboxylic acid binding
Biological process
Cellular component
Molecular function
E
hsa05200:Pathways in cancer
hsa04933:AGE−RAGE signaling pathway in diabetic complications
hsa05418:Fluid shear stress and atherosclerosis
hsa05417:Lipid and atherosclerosis
hsa05205:Proteoglycans in cancer
hsa05163:Human cytomegalovirus infection
hsa05215:Prostate cancer
hsa05161:Hepatitis B
hsa04668:TNF signaling pathway
hsa05208:Chemical carcinogenesis − reactive oxygen species
hsa05167:Kaposi sarcoma−associated herpesvirus infection
hsa04151:PI3K−Akt signaling pathway
hsa04010:MAPK signaling pathway
hsa05145:Toxoplasmosis
hsa05135:Yersinia infection
hsa01522:Endocrine resistance
hsa04926:Relaxin signaling pathway
hsa05212:Pancreatic cancer
hsa04625:C−type lectin receptor signaling pathway
hsa05140:Leishmaniasis
Description
20
30
40
Enrichment
−log10(pvalue)
70
60
50
40
30
count
30
40
50
60
70

Figure 5. Network pharmacology results. A. Venn diagram of atherosclerotic disease targets versus SGF therapeutic targets from OMIN, DiSGeNET, and GeneCards databases. B. The PPI network diagram of 243 potential targets for treating atherosclerosis with the Shenzhu Guanxin Formula. C. The anti-atherosclerosis critical targets of SGF. The orange central area indicates the top 15 out of the 60 key targets. D. GO enrichment analysis of potential therapeutic targets of SGF for atherosclerosis. The top 10 GO terms in BP, MF and CC were shown. E. Conducted a top 20 KEGG enrichment pathway analysis on the potential targets of SGF in the treatment of atherosclerosis.

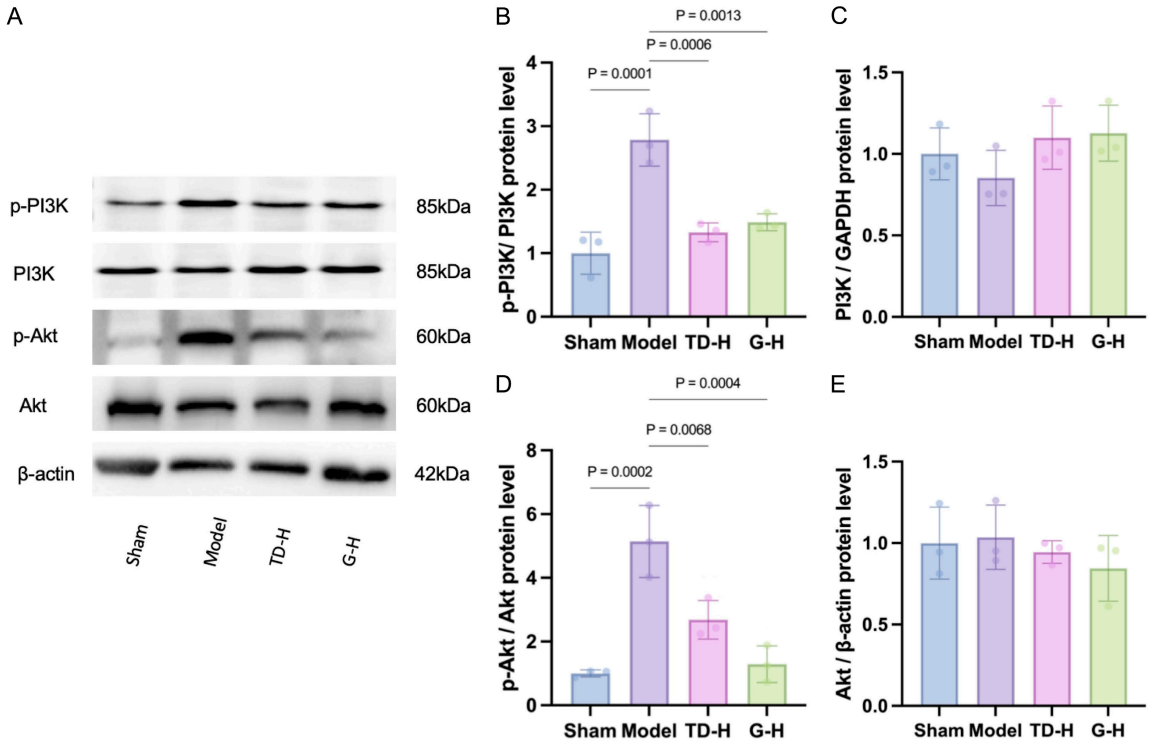

Figure 6. SGF selectively inhibits the protein levels of p-PI3K and p-Akt in the arteries of atherosclerosis models without affecting the total protein levels. A. Representative immunoblots of p-PI3K, p-Akt, PI3K and Akt. B-E. Protein semi-quantitative analysis normalized to internal references ($\overline{x}\pm s$, n=3). Note: G-H, G-M, G-L: High/Medium/Low dose granule of SGF.

production in HUVECs ($P < 0.0001$; **Figure 7D**, **7E**); this antioxidant effect was abolished by co-treatment with the Akt agonist Sc79 (**Figure 7E**).

SGF exerts anti-atherosclerotic effects through the PI3K/Akt pathway

After treating cells with 75 μg/mL oxLDL for 24 hours, western blot analysis showed an increase in the expression levels of p-PI3K and p-Akt proteins in HUVECs ($P < 0.05$; **Figure 7F**, **7G**). However, treatment with serum containing SGF, the phosphorylation activation of the PI3K/Akt pathway was inhibited without altering the total protein levels ($P < 0.05$; **Figure 7G**). Notably, this inhibitory effect was counteracted after pretreatment with 10 μM Sc79 (an Akt agonist) for 2 hours (**Figure 7G**).

Discussion

Atherosclerosis features platelet aggregation and vulnerable plaques, whose rupture initiates thrombosis and subsequent cardiovascular or cerebrovascular diseases such as myocardial and cerebral infarction [21]. The pathogenesis of AS is driven by interconnected pathological processes: dyslipidemia, chronic inflammation, oxidative stress, and endothelial injury, which form a feedforward loop to promote lesion initiation and progression [22, 23].

The rat AS model established in this study, combining a high-fat diet, vitamin D_3 injection, and carotid artery clamping, has strong clinical translational relevance. Unlike single-factor high-fat models, this "three-hit" model simultaneously recapitulates three core pathological

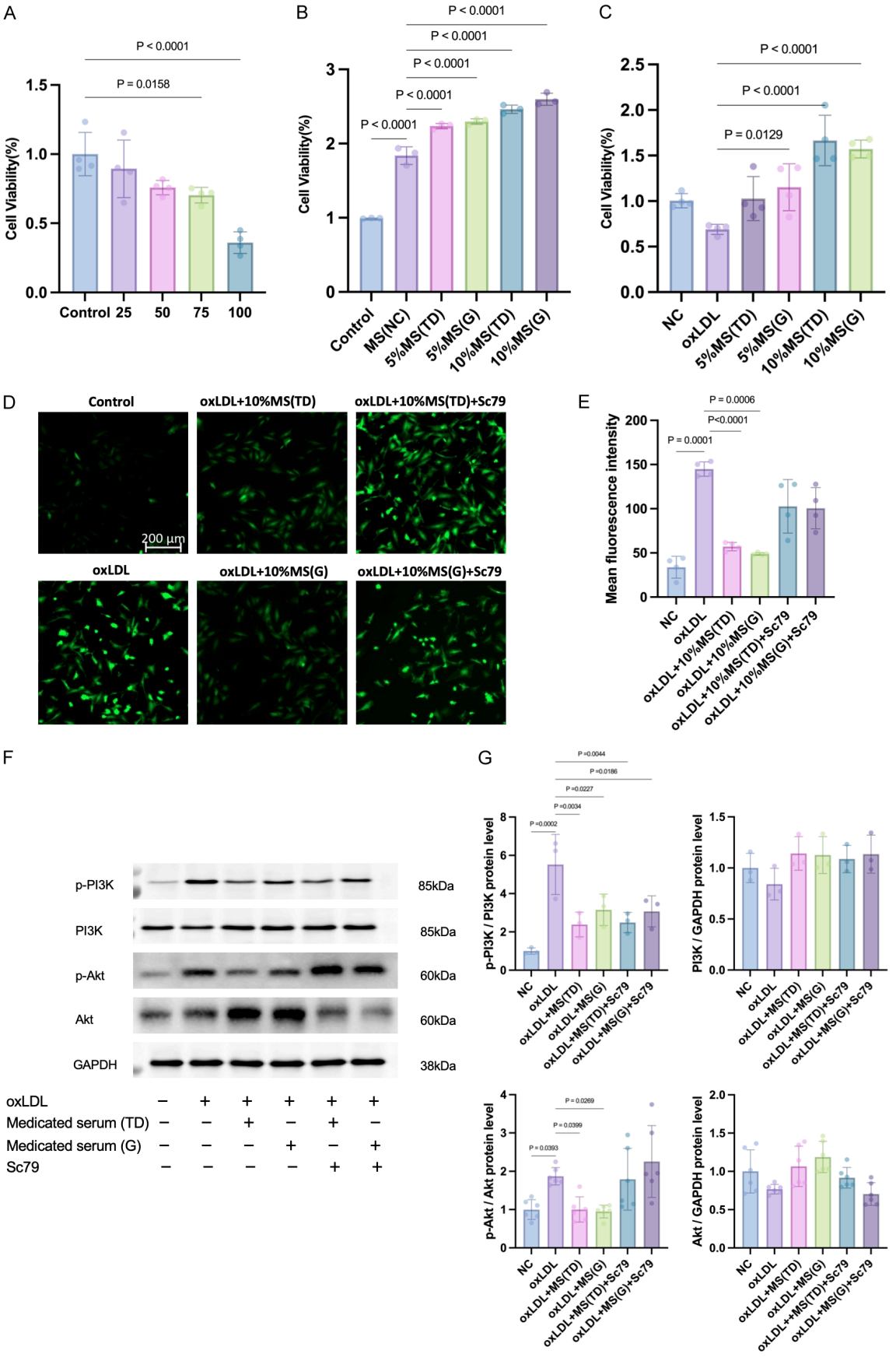
A
P < 0.0001
P = 0.0158
Cell Viability(%)
Control 25 50 75 100
B
P < 0.0001
P < 0.0001
P < 0.0001
P < 0.0001
P < 0.0001
Cell Viability(%)
Control MS(NC) 5%MS(TD) 5%MS(G) 10%MS(TD) 10%MS(G)
C
P < 0.0001
P < 0.0001
P = 0.0129
Cell Viability(%)
NC oxLDL 5%MS(TD) 5%MS(G) 10%MS(TD) 10%MS(G)
D
Control
oxLDL+10%MS(TD)
oxLDL+10%MS(TD)+Sc79
200 μm
oxLDL
oxLDL+10%MS(G)
oxLDL+10%MS(G)+Sc79
E
P = 0.0006
P<0.0001
P = 0.0001
Mean fluorescence intensity
NC oxLDL oxLDL+10%MS(TD) oxLDL+10%MS(G) oxLDL+10%MS(TD)+Sc79 oxLDL+10%MS(G)+Sc79
F
p-PI3K 85kDa
PI3K 85kDa
p-Akt 60kDa
Akt 60kDa
GAPDH 38kDa
oxLDL – + + + + +
Medicated serum (TD) – – + – + –
Medicated serum (G) – – – + – +
Sc79 – – – – + +
G
P =0.0044
P =0.0186
P =0.0227
P =0.0034
P =0.0002
p-PI3K / PI3K protein level
PI3K / GAPDH protein level
P = 0.0269
P = 0.0399
P = 0.0393
p-Akt / Akt protein level
Akt / GAPDH protein level
NC oxLDL oxLDL+MS(TD) oxLDL+MS(G) oxLDL+MS(TD)+Sc79 oxLDL+MS(G)+Sc79

Figure 7. SGF reversed oxLDL-induced HUVECs' cytotoxicity and intracellular ROS ($\bar{x} \pm s$, $n \geq 3$), and can inhibit the upregulation of p-PI3K and p-Akt protein expression in HUVECs induced by oxLDL-induced damage, and this effect can be reversed by Sc79. A. Cell viability of HUVECs after being continuously cultured for 24 hours with 10% drug-free serum, 5% or 10% drug serum containing SGF in the form of decoction or granules. B. The viability of HUVECs after being treated with oxLDL at concentrations ranging from 0 to 100 μg/mL for 24 hours. C. HUVECs were divided into NC (10% concentrations of no medicated serum), oxLDL, 5% or 10% concentrations of medicated serum SGF decoction or granule cultured for 24 h, then cell viability was assessed. D. Representative image of the ROS fluorescence experiment. E. Quantitative analysis of intracellular fluorescence intensity. F. Representative graphs of p-PI3K, PI3K, p-Akt and Akt. G. p-PI3K, PI3K, p-Akt and Akt protein semi-quantitative analysis normalized to internal reference protein ($\bar{x} \pm s$, $n \geq 3$). MS (TD), MS (G): The medicated serum extracted from rats by gavage of traditional decoctions and granules of SGF.

features of human AS: systemic dyslipidemia, vascular calcification, and hemodynamic disturbance-induced local endothelial injury. It enables rapid formation of stable atherosclerotic lesions without the long breeding cycle of genetically modified models, providing a robust and clinically relevant in vivo system for evaluating SGF's anti-AS efficacy.

Dyslipidemia, hepatic steatosis, and hemodynamic impairment are interconnected drivers of atherosclerosis [2, 24-26]. The ability of SGF to improve serum lipids, hepatic lipid deposition, and carotid blood flow suggests a coordinated effect on systemic lipid metabolism and vascular function. By reducing circulating lipid levels, SGF likely lowers blood viscosity and attenuates apolipoprotein deposition on damaged endothelium, thereby preserving endothelial integrity and hemodynamic competence [24, 26].

Chronic inflammation and oxidative stress jointly propel atherogenesis. Pro-inflammatory cytokines such as TNF-α, IL-1β, and IL-6 promote endothelial activation and plaque progression [27], and their downregulation by SGF therefore represents a critical anti-atherosclerotic mechanism. Concurrently, SGF restored antioxidant defenses - evidenced by increased arterial SOD and GSH levels in vivo and suppressed oxLDL-induced ROS production in HUVECs - counteracting the lipid peroxidation and endothelial injury that drive disease progression [28, 29]. These findings indicate that SGF breaks the feed-forward loop between oxidative damage and vascular inflammation.

Endothelial dysfunction is a central event throughout the entire course of AS. The downregulation of eNOS impairs vasodilation and anti-inflammatory defense, while the upregulation of ICAM-1, VCAM-1 and VEGF-A promotes monocyte infiltration, pathological neovascularization, and plaque instability [30-32]. The reversal of these endothelial injury markers by SGF demonstrates that it protects vascular endothelial integrity, thereby blocking the progression from early endothelial damage to advanced atherosclerotic lesions.

Network pharmacology identified 99 bioactive components of SGF, with core active compounds including naringenin, quercetin, ginsenoside Rh2, and nobiletin - all of which have been reported to alleviate AS via multi-targeted modulation of lipid metabolism, inflammation, and endothelial integrity [33-36]. Among the identified key targets, core hub genes converge on a functional module driving core AS pathological processes: pro-inflammatory cytokines (IL-1β, IL-6, TNF), signaling kinases and transcription factors (AKT1, NF-κB1, STAT3) [37, 38], and vascular injury response mediators (PPARG, TGF-β1, MMP9) [39, 40]. This module is closely associated with sustained vascular inflammation, endothelial activation, and plaque instability, which aligns perfectly with the anti-inflammatory, endothelial-protective, and plaque-stabilizing effects of SGF observed in our in vivo experiments. To avoid analytical bias from single-method approaches and better fit the multi-target, multi-pathway regulatory characteristics of TCM compounds, we adopted an orthogonal analytical strategy combining network pharmacology prediction with in vivo carotid artery transcriptomic profiling of AS rats after SGF intervention. Notably, this dual-omics analysis revealed robust convergence on the PI3K/Akt signaling pathway. As a canonical phosphorylation cascade, the PI3K/Akt pathway regulates all key AS pathological hallmarks observed in our study, including endothelial dysfunction, lipid metabolism disorders, inflammatory response, and vascular remodeling [41, 42]. This consistent convergence from two independent analytical approaches provides rigorous preclinical rationale for selecting the

PI3K/Akt pathway as the core mechanistic target for subsequent experimental validation.

For TCM clinical translation, the equivalence between traditional decoctions and modern formula granules is a core concern. Decoctions are the classic TCM dosage form with high flexibility for syndrome differentiation, but they have limitations of inconvenient preparation and poor portability. Formula granules, produced by standardized modern extraction and granulation processes, overcome these limitations while retaining the core principles of TCM prescription [43]. This study is the first to demonstrate that SGF decoction and granules exert equivalent anti-AS efficacy in rats, with comparable modulation of lipid profiles, inflammation, oxidative stress, endothelial function, and the core PI3K/Akt regulatory pathway. This finding provides robust preclinical evidence for the clinical promotion and standardized application of SGF granules.

Some limitations exist in this research that warrant consideration. Firstly, these findings are based on a rat AS model, which does not fully recapitulate the complex immune and metabolic intricacies of human disease. Additionally, the study lacks a systematic assessment of long-term toxicity, and the bioactive constituents of SGF along with their downstream pathways require further elucidation.

In conclusion, this study demonstrates that both SGF granules and traditional decoctions attenuate atherosclerosis in rats induced by a high-fat diet, vitamin D_3, and vascular injury, primarily through inhibition of PI3K/Akt signaling. In vitro, SGF reduced oxLDL-induced ROS production and suppressed PI3K/Akt activation. In addition, 99 active components and 60 core targets associated with the anti-atherosclerotic effects of SGF were identified. Overall, these findings provide mechanistic insight into the therapeutic effects of SGF and offer experimental support for the biological equivalence between TCM formula granules and traditional decoctions.

Acknowledgements

This research was funded by grants provided by the Guangdong Basic and Applied Basic Research Foundation (2023A1515220199, 2024A1515220088); National Natural Science Foundation of China (No. 81070125, 81270213, 81670306); the Futian District Health and Public Welfare Research Project of Shenzhen City (No. FTWS2022018, FTWS2023064), the Shenzhen Science and Technology Program (No. JCYJ20220530144404009, KCXFZ20230731094100002); Sanming Project of Medicine in Shenzhen (No. SZSM202402020).

Disclosure of conflict of interest

None.

Address correspondence to: Dr. Tong Wang, Department of Emergency, The Eighth Affiliated Hospital of Sun Yat-sen University, No. 3025 Shennan Middle Road, Futian District, Shenzhen 518003, Guangdong, P. R. China. Tel: +86-13826179957; E-mail: tongwang316@163.com; Dr. Danping Xu, Department of Chinese Medicine, The Eighth Affiliated Hospital of Sun Yat-sen University, No. 3025 Shennan Middle Road, Futian District, Shenzhen 518003, Guangdong, P. R. China. Tel: +86-13826406099; E-mail: xudanping@hotmail.com

References

[1] Młynarska E, Czarnik W, Fularski P, Hajdys J, Majchrowicz G, Stabrawa M, Rysz J and Franczyk B. From atherosclerotic plaque to myocardial infarction-The leading cause of coronary artery occlusion. Int J Mol Sci 2024; 25: 7295.

[2] Li S, Xu Z, Wang Y, Chen L, Wang X, Zhou Y, Lei D, Zang G and Wang G. Recent advances of mechanosensitive genes in vascular endothelial cells for the formation and treatment of atherosclerosis. Genes Dis 2023; 11: 101046.

[3] Gusev E and Sarapultsev A. Atherosclerosis and Inflammation: insights from the theory of general pathological processes. Int J Mol Sci 2023; 24: 7910.

[4] Lordan R, Tsoupras A and Zabetakis I. Platelet activation and prothrombotic mediators at the nexus of inflammation and atherosclerosis: potential role of antiplatelet agents. Blood Rev 2021; 45: 100694.

[5] Wang C, Niimi M, Watanabe T, Wang Y, Liang J and Fan J. Treatment of atherosclerosis by traditional Chinese medicine: questions and quandaries. Atherosclerosis 2018; 277: 136-144.

[6] Liang Y, Liu J, Zhang C, Cheng J, Lu F, Chen P and Liu S. Integrating serum pharmacochemistry and metabolomics to reveal the potential effective ingredients and mechanism of Huangqi Chifeng Tang intervening carotid atherosclerosis. J Ethnopharmacol 2025; 351: 120065.

[7] Kong Z, Sun P, Lu Y, Yang Y, Min DY, Zheng SC, Yang Y, Zhang Z, Yang GL and Jiang JW. Yi Mai granule improve energy supply of endothelial cells in atherosclerosis via miRNA-125a-5p regulating mitochondrial autophagy through Pink1-Mfn2-Parkin pathway. J Ethnopharmacol 2024; 319: 117114.
[8] Wu M, Liu L, Xing Y, Yang S, Li H and Cao Y. Roles and mechanisms of hawthorn and its extracts on atherosclerosis: a review. Front Pharmacol 2020; 11: 118.
[9] Zhu Q, Kang J, Xu G, Li J, Zhou H and Liu Y. Traditional Chinese medicine Shenqi compound to improve lower extremity atherosclerosis of patients with type 2 diabetes by affecting blood glucose fluctuation: study protocol for a randomized controlled multicenter trial. Medicine (Baltimore) 2020; 99: e19501.
[10] Xu DP, Wu HL, Lan TH, Wang X, Sheng XG, Lin Y, Li S and Zheng CY. Effect of Shenzhu Guanxin Recipe () on patients with angina pectoris after percutaneous coronary intervention: a prospective, randomized controlled trial. Chin J Integr Med 2015; 21: 408-416.
[11] Jin X, Wu B, Lin M, Zhong B, Lin L and Xu D. Clinical efficacy and gene chip expression analysis of Shenzhu Guanxin recipe granules in patients with intermediate coronary lesions. J Tradit Chin Med 2024; 44: 545-553.
[12] Mao S, Xu DP, Dang XJ, Li W and Wu HL. Shenzhu Guanxin recipe granules () for improving exercise tolerance in patients with stable angina (SERIES Trial): a protocol of multicenter, randomized, double-blind, placebo parallel controlled clinical trial. Chin J Integr Med 2019; 25: 96-102.
[13] Jin X, Pan B, Wu H, Wu B, Li Y, Wang X, Liu G, Dang X and Xu D. The efficacy and safety of Shenzhu Guanxin recipe granules for the treatment of patients with coronary artery disease: protocol for a double-blind, randomized controlled trial. Trials 2019; 20: 520.
[14] Huang M, Wu H, Wu J, Chen Q, Zou D and Xu D. Prevention of platelet aggregation and arterial thrombosis using a modified Shenzhu Guanxin formula. J Int Med Res 2020; 48: 300060520941326.
[15] Xu DP, Zou DZ, Qiu HL and Wu HL. Traditional Chinese Medicine ShenZhuGuanXin granules mitigate cardiac dysfunction and promote myocardium angiogenesis in myocardial infarction rats by upregulating PECAM-1/CD31 and VEGF expression. Evid Based Complement Alternat Med 2017; 2017: 5261729.
[16] Hu Y, Wang Z, Ni K and Yang J. Challenges in Traditional Chinese Medicine clinical trials: how to balance personalized treatment and standardized research? Ther Clin Risk Manag 2025, 21: 1085-1094.
[17] Zhang C, Hu H, Shi M, Ma Y, Fauci AJ, Lee MS, Wu X, Zhang J and Ji Z. Commercial Chinese polyherbal preparation: current status and future perspectives. Front Pharmacol 2024; 15: 1404259.
[18] Zhang CY, Li XX, Li P, Jiang Y and Li HJ. Consistency evaluation between dispensing granule and traditional decoction from Coptidis Rhizoma by using an integrated quality-based strategy. Phytochem Anal 2021; 32: 153-164.
[19] Huang X, Liu X, Lin X, Yuan Z, Zhang Y, Wang Z, Pi W, Zhao H, Lei H and Wang P. Thermodynamics driving phytochemical self-assembly morphological change and efficacy enhancement originated from single and co-decoction of traditional Chinese medicine. J Nanobiotechnology 2022; 20: 527.
[20] Wojcikowski K and Gobe G. Animal studies on medicinal herbs: predictability, dose conversion and potential value. Phytother Res 2014; 28: 22-27.
[21] Baaten CCFMJ, Nagy M, Bergmeier W, Spronk HMH and van der Meijden PEJ. Platelet biology and function: plaque erosion vs. rupture. Eur Heart J 2024; 45: 18-31.
[22] Yuan D, Chu J, Lin H, Zhu G, Qian J, Yu Y, Yao T, Ping F, Chen F and Liu X. Mechanism of homocysteine-mediated endothelial injury and its consequences for atherosclerosis. Front Cardiovasc Med 2023; 9: 1109445.
[23] Vekic J, Stromsnes K, Mazzalai S, Zeljkovic A, Rizzo M and Gambini J. Oxidative stress, atherogenic dyslipidemia, and cardiovascular risk. Biomedicines 2023; 11: 2897.
[24] Higashi Y. Endothelial function in dyslipidemia: roles of LDL-cholesterol, HDL-cholesterol and triglycerides. Cells 2023; 12: 1293.
[25] Li H, Yu XH, Ou X, Ouyang XP and Tang CK. Hepatic cholesterol transport and its role in non-alcoholic fatty liver disease and atherosclerosis. Prog Lipid Res 2021; 83: 101109.
[26] Fukuda S, Shimogonya Y, Watanabe A, Yoshimoto Y, Maruyama S, Yonemoto N, Fujiwara K, Fukuda M and Yasoda A; NHO Carotid CFD Study Group. Hemodynamic environments for the progression of carotid stenosis: the NHO carotid CFD study. Arterioscler Thromb Vasc Biol 2025; 45: 1448-1458.
[27] Xing Y and Lin X. Challenges and advances in the management of inflammation in atherosclerosis. J Adv Res 2025; 71: 317-335.
[28] Marchio P, Guerra-Ojeda S, Vila JM, Aldasoro M, Victor VM and Mauricio MD. Targeting early atherosclerosis: a focus on oxidative stress and inflammation. Oxid Med Cell Longev 2019; 2019: 8563845.
[29] Yan R, Zhang X, Xu W, Li J, Sun Y, Cui S, Xu R, Li W, Jiao L and Wang T. ROS-induced endothelial dysfunction in the pathogenesis of atherosclerosis. Aging Dis 2024; 16: 250-268.

[30] Janaszak-Jasiecka A, Płoska A, Wierońska JM, Dobrucki LW and Kalinowski L. Endothelial dysfunction due to eNOS uncoupling: molecular mechanisms as potential therapeutic targets. Cell Mol Biol Lett 2023; 28: 21.
[31] Bei YR, Zhang SC, Song Y, Tang ML, Zhang KL, Jiang M, He RC, Wu SG, Liu XH, Wu LM, Dai XY and Hu YW. EPSTI1 promotes monocyte adhesion to endothelial cells in vitro via upregulating VCAM-1 and ICAM-1 expression. Acta Pharmacologica Sinica 2023; 44: 71-80.
[32] Guo L, Akahori H, Harari E, Smith SL, Polavarapu R, Karmali V, Otsuka F, Gannon RL, Braumann RE, Dickinson MH, Gupta A, Jenkins AL, Lipinski MJ, Kim J, Chhour P, de Vries PS, Jinnouchi H, Kutys R, Mori H, Kutyna MD, Torii S, Sakamoto A, Choi CU, Cheng Q, Grove ML, Sawan MA, Zhang Y, Cao Y, Kolodgie FD, Cormode DP, Arking DE, Boerwinkle E, Morrison AC, Erdmann J, Sotoodehnia N, Virmani R and Finn AV. CD163+ macrophages promote angiogenesis and vascular permeability accompanied by inflammation in atherosclerosis. J Clin Invest 2018; 128: 1106-1124.
[33] Adetunji JA, Fasae KD, Awe AI, Paimo OK, Adegoke AM, Akintunde JK and Sekhoacha MP. The protective roles of citrus flavonoids, naringenin, and naringin on endothelial cell dysfunction in diseases. Heliyon 2023; 9: e17166.
[34] Ebrahimi F, Ghazimoradi MM, Fatima G and Bahramsoltani R. Citrus flavonoids and adhesion molecules: potential role in the management of atherosclerosis. Heliyon 2023; 9: e21849.
[35] Wang YM, Chu TJ, Wan RT, Niu WP, Bian YF and Li J. Quercetin ameliorates atherosclerosis by inhibiting inflammation of vascular endothelial cells via Piezo1 channels. Phytomedicine 2024; 132: 155865.
[36] Sun JL, Abd El-Aty AM, Jeong JH and Jung TW. Ginsenoside Rb2 ameliorates LPS-induced inflammation and ER stress in HUVECs and THP-1 cells via the AMPK-mediated pathway. Am J Chin Med 2020; 48: 967-985.
[37] Ageeva T, Rizvanov A and Mukhamedshina Y. NF-κB and JAK/STAT signaling pathways as crucial regulators of neuroinflammation and astrocyte modulation in spinal cord injury. Cells 2024; 13: 581.
[38] Li C, Wang Q, Dai F, Xiang X, Yi L, Shao B, Li Q, Peng X, Li R, Luo F, Wu Z and Xiang T. NKAPL suppresses NSCLC progression by enhancing the protein stability of TRIM21 and further inhibiting the NF-κB signaling pathway. Genes Dis 2025; 12: 101598.
[39] Zheng Y, Shao M, Zheng Y, Sun W, Qin S, Sun Z, Zhu L, Guan Y, Wang Q, Wang Y and Li L. PPARs in atherosclerosis: the spatial and temporal features from mechanism to druggable targets. J Adv Res 2025; 69: 225-244.
[40] Low EL, Baker AH and Bradshaw AC. TGFβ, smooth muscle cells and coronary artery disease: a review. Cell Signal 2019; 53: 90-101.
[41] Wu B, Li C, Luo X, Kan H, Li Y, Zhang Y, Rao X, Zhao P and Liu Y. Identification of key hypolipidemic components and exploration of the potential mechanism of total flavonoids from rosa sterilis based on network pharmacology, molecular docking, and zebrafish experiment. Curr Issues Mol Biol 2024; 46: 5131-5146.
[42] Zhu L, Chen Q, Wang B, Fu J, Liu Z, Cui Y, Zhang R, Liu F, Niu S and Zhou Y. PI3K/AKT signaling pathway: new strategies for treating atherosclerosis with plant-derived compounds. Front Pharmacol 2026; 17: 1722493.
[43] Qin LL, Yu M, Zhang HX, Jia HM, Ye XC and Zou ZM. Quality markers of Baizhu dispensing granules based on multi-component qualitative and quantitative analysis combined with network pharmacology and chemometric analysis. J Ethnopharmacol 2022; 288: 114968.

Appendix 1. The active components of SGF were screened by network pharmacology

Serial Number	Name
1	sitosterol
2	naringenin
3	5,7-dihydroxy-2-(3-hydroxy-4-methoxyphenyl)chroman-4-one
4	Citromitin
5	nobiletin
6	Diop
7	Stigmasterol
8	beta-sitosterol
9	Chrysanthemaxanthin
10	arachidonate
11	ginsenoside rh2
12	Inermin
13	kaempferol
14	Aposiopolamine
15	Deoxyharringtonine
16	Dianthramine
17	Frutinone A
18	Girinimbin
19	Panaxadiol
20	Fumarine
21	suchilactone
22	(3S,8S,9S,10R,13R,14S,17R)-10,13-dimethyl-17-[(2R,5S)-5-propan-2-yloctan-2-yl]-2,3,4,7,8,9,11,12,14,15,16,17-dodecahydro-1H-cyclopenta[a]phenanthren-3-ol
23	3β-acetoxyatractylone
24	8β-ethoxy atractylenolide III
25	Mandenol
26	DFV
27	ginsenoside f2
28	quercetin
29	24-Ethylcholest-4-en-3-one
30	Cavidine
31	baicalein
32	Baicalin
33	gondoic acid
34	coniferin
35	Cycloartenol
36	beta-D-Ribofuranoside, xanthine-9
37	crocetin
38	croomionidine
39	genipinic acid
40	methyl(2e,8z)-decadien-4,6-diynoate
41	ursolic acid
42	hirudin
43	stigmast-7-enol
44	papaverine
45	(8S,9S,10R,13R,14S,17R)-17-[(1R,4R)-4-ethyl-1,5-dimethylhexyl]-10,13-dimethyl-1,2,8,9,11,12,14,15,16,17-decahydrocyclopenta[a]phenanthren-7-one

46	(2R,3S,4S,5R,6R)-2-(hydroxymethyl)-6-[[(3S,5R,8R,9R,10R,12R,13R,14R,17S)-12-hydroxy-4,4,8,10,14-pentamethyl-17-[(2S)-6-methyl-2-[(2S,3R,4S,5S,6R)-3,4,5-trihydroxy-6-(hydroxymethyl)oxan-2-yl]oxyhept-5-en-2-yl]-2,3,5,6,7,9,11,12,13,15,16,17-dodecahydro-1H-c
47	poncirin
48	Isosinensetin
49	5,7,4'-Trimethylapigenin
50	neohesperidin_qt
51	Sinensetin
52	didymin
53	formyltanshinone
54	Poriferasterol
55	poriferast-5-en-3beta-ol
56	isoimperatorin
57	Dehydrotanshinone II A
58	digallate
59	luteolin
60	α-amyrin
61	5,6-dihydroxy-7-isopropyl-1,1-dimethyl-2,3-dihydrophenanthren-4-one
62	2-isopropyl-8-methylphenanthrene-3,4-dione
63	3α-hydroxytanshinoneIIa
64	(E)-3-[2-(3,4-dihydroxyphenyl)-7-hydroxy-benzofuran-4-yl]acrylic acid
65	4-methylenemiltirone
66	2-(4-hydroxy-3-methoxyphenyl)-5-(3-hydroxypropyl)-7-methoxy-3-benzofurancarboxaldehyde
67	neocryptotanshinone ii
68	salvianolic acid j
69	sugiol
70	3-beta-Hydroxymethyllenetanshiquinone
71	Methylenetanshinquinone
72	przewalskin b
73	Przewaquinone B
74	przewaquinone c
75	(6S,7R)-6,7-dihydroxy-1,6-dimethyl-8,9-dihydro-7H-naphtho[8,7-g]benzofuran-10,11-dione
76	przewaquinone f
77	sclareol
78	tanshinaldehyde
79	Danshenol B
80	Danshenol A
81	Salvilenone
82	cryptotanshinone
83	deoxyneocryptotanshinone
84	C09092
85	isocryptotanshi-none
86	Isotanshinone II
87	miltionone I
88	miltionone II
89	miltipolone
90	Miltirone
91	neocryptotanshinone
92	1-methyl-8,9-dihydro-7H-naphtho[5,6-g]benzofuran-6,10,11-trione

93	salvianolic acid g
94	salviolone
95	Tanshindiol B
96	Przewaquinone E
97	tanshinone iia
98	(6S)-6-(hydroxymethyl)-1,6-dimethyl-8,9-dihydro-7H-naphtho[8,7-g]benzofuran-10,11-dione
99	tanshinone VI